

Imaging changes in blood volume and oxygenation in the newborn infant brain using three-dimensional optical tomography

Jeremy C Hebden¹, Adam Gibson¹, Topun Austin³, Rozarina Md Yusof¹, Nick Everdell¹, David T Delpy¹, Simon R Arridge², Judith H Meek³ and John S Wyatt³

¹ Department of Medical Physics and Bioengineering, University College London, 11-20 Capper Street, London WC1E 6JA, UK

² Department of Computer Science, University College London, Gower Street, London WC1E 6BT, UK

³ Department of Paediatrics and Child Health, University College London, 5 University Street, London WC1E 6JJ, UK

Received 16 October 2003

Published 18 March 2004

Online at stacks.iop.org/PMB/49/1117 (DOI: 10.1088/0031-9155/49/7/003)

Abstract

Induced haemodynamic and blood oxygenation changes occurring within the brain of a ventilated newborn infant have been imaged in three dimensions using optical tomography. Noninvasive measurements of the flight times of transmitted light were acquired during illumination of the brain by laser pulses at wavelengths of 780 nm and 815 nm. The oxygen and carbon dioxide partial pressures were adjusted through alterations to the ventilator settings, resulting in changes to the cerebral blood volume and oxygenation. Three-dimensional images were generated using the physiologically associated differences in the measured data, obviating the need for data calibration using a separate reference measurement. The results exhibit large changes in absorption coefficient at both wavelengths. Images corresponding to differences in concentrations of oxy- and deoxyhaemoglobin are in qualitative agreement with known physiological data.

1. Introduction

Since Jöbsis (1977) first reported that near-infrared spectroscopy (NIRS) could be used to monitor cerebral oxygenation and haemodynamics noninvasively, the technique has evolved into an important research tool with a variety of clinical applications. Simultaneous monitoring of the transmittance across the brain at two or more wavelengths enables changes in attenuation to be converted into changes in the cerebral concentrations of oxyhaemoglobin $\Delta[\text{HbO}_2]$ and deoxyhaemoglobin $\Delta[\text{Hb}]$, which then yield the mean cerebral oxygen saturation, SmcO_2 . The

change in total haemoglobin concentration $\Delta[\text{Hb}_{\text{tot}}] = \Delta[\text{Hb}] + \Delta[\text{HbO}_2]$ can therefore be derived, which is directly related to the change in cerebral blood volume (ΔCBV). Increasing the number of wavelengths enables changes in the concentrations of other chromophores, such as cytochrome, to be also taken into account. One of the first reported uses of NIRS to study the cerebral oxygenation of newborn infants was that described by Brazy *et al* (1985), who measured changes in both haemoglobin and cytochrome aa_3 absorption. NIRS is a highly attractive technique because of its facility to monitor infants in intensive care safely and continuously. Of particular interest is the study of infants suspected of having suffered hypoxic-ischaemic brain injury, which lacks sufficiently reliable methods of early diagnosis and treatment, and which can lead to permanent disability. Measurements of various global oxygenation and haemodynamic parameters have been performed using NIRS on newborn infants, including changes in $[\text{Hb}]$, $[\text{HbO}_2]$, $[\text{Hb}_{\text{tot}}]$, CBV and cerebral blood flow (CBF) (Reynolds *et al* 1988, Edwards *et al* 1988, Skov *et al* 1991, Wyatt 1993, Meek *et al* 1999, Isobe *et al* 2000, Tsuji *et al* 2000).

The desire to determine the spatial variation of chromophore concentrations within tissue has led to the development of near-infrared imaging techniques, involving measurement of transmitted light at multiple sites on the surface of the head. The application of such techniques to imaging the newborn infant brain has recently been reviewed by Hebden (2003). Two distinct approaches have been developed. Optical topography is a surface mapping technique which involves acquiring multiple measurements of diffuse reflectance at small source–detector separations over a large area of the head. By keeping the separation low, measured signals are relatively high and therefore may be acquired quickly, enabling fast haemodynamic changes within the outer (cortical) regions of the brain to be studied. Recently several groups have performed topography studies on infants in order to observe the cerebral haemodynamic response to sensory stimuli (Chance *et al* 1998, Hintz *et al* 2001, Isobe *et al* 2001). A second approach, known as optical tomography, involves generating images of the entire three-dimensional (3D) volume. Measurements must be made at large source–detector separations to achieve adequate sensitivity to deeper tissues, which requires longer imaging times. As a consequence, optical tomography is less useful for analysing fast haemodynamic phenomena, but enables long-term changes to be monitored over a period of hours or days. Imaging systems acquire measurements of transmitted light between pairs of points on the surface of an object, and a suitable algorithm is used to convert these data into a transverse slice or 3D volume representing the distribution of internal optical properties. The first successful attempt to image the infant brain using optical tomography was reported by Benaron and colleagues at Stanford (Benaron *et al* 2000, Hintz *et al* 1998), who have built an imaging system which measures photon flight times between points around the circumference of the infant head. Despite long scan times (between 2 and 6 h) resulting from a low source power (100 μW average), and a relatively unsophisticated image reconstruction algorithm, cross-sectional images were acquired which revealed incidence of intracranial haemorrhage (Hintz *et al* 1998, 1999), and regions of low oxygenation after acute stroke (Benaron *et al* 2000).

In 2002 our group acquired the first 3D optical tomography images of the infant brain (Hebden *et al* 2002). Scan times of less than 10 min were achieved using a 32-channel imaging system described in section 2. Image reconstruction was performed using a sophisticated diffusion-based nonlinear algorithm known as TOAST (temporal optical absorption and scattering tomography) which has been developed at UCL by Arridge and Schweiger (1997). TOAST compares measured datatypes (representing specific characteristics of the transmitted signal) with the predictions of a finite element method (FEM) forward model of the investigated tissue to iteratively update the parameters of the model until an acceptable match is achieved

(Arridge 1999). Two 3D images are generated representing the internal distributions of the absorption coefficient μ_a , and the transport scatter coefficient μ'_s . Absorption images of the brain of a premature infant with a cerebral haemorrhage predominantly located within the left ventricle revealed an asymmetry consistent with an ultrasound examination.

In some respects the preterm infant is an ideal subject for near-infrared spectroscopy and imaging. Extremely preterm infants are less likely to move, causing fewer motion-induced artefacts, and the thinness of their skulls provides a high penetration of light into the brain. These infants are often mechanically ventilated, which facilitates controlled manipulation of physiological variables such as partial pressures of carbon dioxide (PaCO₂) and oxygen (PaO₂). In this paper we report the changes displayed in the internal optical properties of the infant brain caused by alterations to ventilator settings. As described below, a difference imaging approach enables images to be generated using integrated intensity information for the first time, and allows images to be reconstructed without recourse to reference measurements on a phantom of known optical properties.

2. Method

2.1. Imaging system

The imaging device designed and built at UCL for performing 3D optical tomography consists of 32 parallel detectors which measure the times-of-flight of transmitted photons at two near-infrared wavelengths simultaneously. The sources are two synchronized fibre lasers (built by IMRA, Inc.) operating at 780 nm and 815 nm, which illuminate the head via a 32-way optical fibre switch. The light transmitted across the tissue is collected by 32 detector fibre bundles, which are coupled to four 8-anode microchannel-plate photomultiplier tubes (MCP-PMTs). The output end of each source fibre (graded index, with 62.5 μm core diameter and 125 μm cladding diameter) is permanently integrated along the central axis of a corresponding detector bundle (approximately three thousand step index fibres with 40 μm core diameter and 50 μm cladding diameter; 3.2 mm diameter). This co-axial arrangement has two major benefits. First, it decreases the number of connectors required to couple 32 sources and 32 detectors to the infant head. Second, it enables back-reflected light at the surface to be used to calibrate the system *in situ*, in a manner described by Hebden *et al* (2003). The detection electronics consists of 32 parallel time-correlated single photon counting (TCSPC) units. A detailed description of the imaging system, known as MONSTIR (multi-channel opto-electronic near-infrared system for time-resolved image reconstruction), is provided in a paper by Schmidt *et al* (2000). The arrival times of the detected photons are measured with respect to a laser-generated reference signal, and histograms of photon flight times (temporal point spread functions, or TPSFs) are accumulated. The full set of TPSFs is subsequently transferred to a dedicated workstation for processing and image reconstruction.

Coupling optical fibres/fibre bundles to the heads of newborn infants, who are usually also premature and/or critically-ill, has proven to be a significant challenge, and we are currently developing improved methods in our laboratory. The solution we have employed to date has been to construct customized helmets for each infant, consisting of two parts made from thermoplastic and soft foam (see Hebden *et al* 2002 for details). The combined source/detector bundles are attached to the helmet using a plastic connector which holds them approximately 10 mm from the skin surface, providing a common circular illumination and detection area with a diameter of 6 mm. This is sufficiently broad to ensure that a moderate amount of hair on the infant head is not an overwhelming influence on the coupling of light into and out of the skin.

2.2. Difference imaging

An essential requirement for image reconstruction using the TOAST algorithm is prior knowledge of the spatial coordinates of all sources and detectors on the head. In practice, the positions of fibres on the helmet are recorded using a 3D digitizing arm (Microscribe 3D, Immersion Corp., USA) immediately before or after a clinical measurement. However, since the helmet structure is necessarily mechanically deformable, the actual positions of fibres on the head are inevitably slightly different. Measuring the positions *during* the scan is currently impractical since the infant's head prevents access to the rear section of the helmet. While image reconstruction is normally very sensitive to error in the source/detector positions, the requirement for accurate positions becomes significantly less severe when reconstructing images using *differences* in data resulting from a *change* in the optical properties. We have therefore previously circumvented this problem by recording a set of data using a homogeneous reference object of known optical properties placed within the same helmet. In practice, a homogeneous phantom is inserted into the helmet immediately following an infant scan, consisting of a balloon filled with a solution of intralipid and near-infrared dye. In this paper, we describe a series of clinical measurements on an infant head where the need for a reference phantom measurement is obviated by inducing changes in the optical properties of the brain. For this new situation, the differences in the optical measurements are employed to generate images which directly reveal the regions of the brain where the changes occurred. The principles and limitations of difference imaging are discussed in detail by Hillman *et al* (2000).

The facility to acquire data consecutively on the same head between induced changes in the internal optical properties provides an additional highly significant benefit for optical tomography. Due to the presence of hair and uncertainty in the skin reflectance, the efficiency of the coupling of light into and out of the infant head is generally almost impossible to quantify. As a consequence, absolute measurements of integrated transmitted intensity cannot be used as a datatype for image reconstruction. Nevertheless, simulations have revealed that a combination of datatypes *including* intensity is highly desirable, and is considered particularly effective for separating the effects of absorption and scatter (Schweiger and Arridge 1999). However, by making an assumption that surface coupling remains constant between consecutive measurements (reasonable for a sleeping or otherwise immobile preterm infant), intensity ratios (or differences in log intensity) provide a highly robust datatype for image reconstruction.

2.3. Clinical measurements

Informed parental consent was obtained to perform a study on a four-day-old female term infant who had suffered a severe global hypoxic-ischaemic insult following uterine rupture. As part of the intensive care of severely asphyxiated infants, she required mechanical ventilation, sedation and muscle relaxants. Prior to the study, a series of digital photographs were taken of her head in order to construct a customized helmet to support 29 source/detector pairs around the top and back hemispheres, as shown in figure 1. The number of sources/detectors was less than the maximum available (32) due to limited space on the surface of the helmet in which to insert the plastic connectors.

Following a period of about 5 min after attaching the helmet to the infant, a set of data was acquired which involved illuminating each source for 15 s while TPSFs were recorded by each detector simultaneously. The ventilator settings during this first 'baseline' measurement corresponded to a PaO₂ of 13.4 kPa and a PaCO₂ of 4.5 kPa. Thereafter a series of datasets



Figure 1. Three-dimensional optical tomography of a ventilated infant.

Table 1. Optical tomography measurements performed on infant at different ventilator settings.

Dataset number	Time (min)	Event	Acquisition time (s per source)	PaO ₂ (kPa)	PaCO ₂ (kPa)
1	0	Baseline measurement 1	15	13.4	4.5
2	15	Increased PaCO ₂	5	14.7	5.5
3	30	Increased PaCO ₂	5	14.0	6.5
4	45	Increased PaCO ₂	5	14.5	7.5
5	80	Increased PaCO ₂	15	16.3	8.0
6	95	Decreased PaO ₂ at peak PaCO ₂	15	8.8	8.0
7	140	Baseline measurement 2	15	13.5	4.6
8	165	Decreased PaO ₂ at baseline PaCO ₂	15	7.1	4.7
	190	Return to baseline		13.4	4.5

were acquired sequentially using shorter acquisition times (5 s per source) as the PaCO₂ was increased in steps up to 8.0 kPa by decreasing the respiration rate. The fraction of inspired oxygen was increased slightly over this time to maintain a constant arterial oxygen saturation. With the PaCO₂ maintained at this level, a further set of data was acquired (using 15 s per source) at a lower value of PaO₂ (8.8 kPa), and then the ventilator settings were returned to approximately the initial levels for another baseline acquisition. A final dataset was then recorded following a decrease of the PaO₂ to 7.1 kPa while maintaining a constant PaCO₂. The full sequence of measurements is given in table 1 and the partial pressures are plotted against time in figure 2.

As the imaging system switched between source positions, the light reaching each detector was automatically attenuated by predefined amounts (and to zero when necessary) to prevent saturation of the MCP-PMTs. Calibration measurements were also performed immediately before and after the acquisition of clinical data, which involved detecting light back-reflected at the skin surface while the source illumination was heavily attenuated (using a filter with a neutral density of 8). These measurements, and prior knowledge of the temporal characteristics

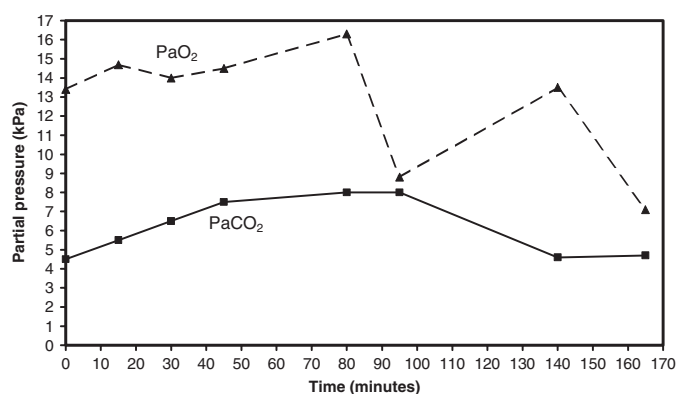


Figure 2. Partial pressures of CO₂ and O₂ measured during the series of optical tomography scans.

Table 2. Datasets used for difference imaging.

Datasets	Difference	Δt (min)	ΔPaO_2 (kPa)	$\Delta PaCO_2$ (kPa)
1 and 7	Difference in baseline measurements	140	+0.1	+0.1
1 and 5	Increase in PaCO ₂ and PaO ₂	80	+2.9	+3.5
5 and 6	Decrease in PaO ₂ at high PaCO ₂	15	-7.5	0.0
7 and 8	Decrease in PaO ₂ at baseline PaCO ₂	25	-6.4	+0.1

of each source fibre, enable a full temporal calibration of the data to be performed (Hebden *et al* 2003). Values of integrated intensity and mean flight time were calculated from each TPSF. Although temporal calibration is not necessary to generate the difference images described below, this process enables erroneous data values (such as due to contamination of signal by ambient light or temporal jitter in the detector electronics) to be easily identified and eliminated prior to image reconstruction.

After the study, a 3D digitizer was used to measure the locations of the sources/detectors on the helmet. Using a process described in detail by Gibson *et al* (2003), a FEM mesh of the infant head was generated by warping a generic infant head surface mesh to the measured coordinates of the sources and detectors, and then using the new surface to construct a volume mesh. The resulting FEM mesh contained 13 871 tetrahedral elements with quadratic interpolation functions having a total of 21 233 nodes. The forward data generated using this mesh were shown to provide positive intensity and mean-time fields everywhere, indicating that the mesh was likely to be numerically stable.

Image reconstruction was performed using selected pairs of datasets at both wavelengths, as listed in table 2. TOAST first calculates the differences between the values of mean flight time and log intensity for each active source–detector combination. The algorithm then employs an iterative procedure to generate 3D distributions (i.e. images) of absorption and scatter which yield forward data as close as possible to the measured difference data added to the forward prediction of an initial estimate. In practice, the initial estimate corresponds to a homogeneous mesh with optical properties of $\mu_{s'} = 1.0 \text{ mm}^{-1}$ and $\mu_a = 0.01 \text{ mm}^{-1}$. It is important to note that the resulting absorption and scatter images are not absolute representations of the infant brain, but reveal how the homogeneous initial estimate must be perturbed in order to reproduce the measured differences in data. Inevitably, the absolute

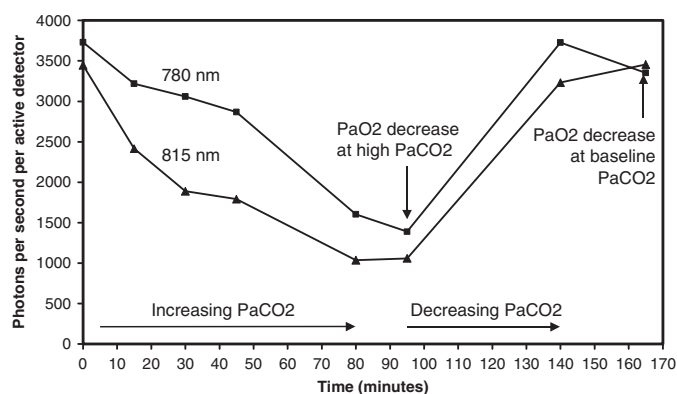


Figure 3. Mean photon detection rates per detector at 780 nm and 815 nm during series of optical tomography scans.

values of these reconstructed ‘difference’ images are highly dependent on the starting values of the initial estimate. Nevertheless, simulations have revealed that the qualitative appearance of these images (and the relative values of reconstructed coefficients) are reasonably independent of the starting values, provided they are ‘sufficiently close’ to the true average values for the head. In principle, the iterative process enables greater tolerance in the selection of starting values. The validity of this so-called perturbation approach is considered further in section 4. For each reconstruction, TOAST performed 20 iterations, although no noticeable improvement in image quality was observed after about the tenth iteration (which is presented below for each case). Each iteration required 7 min on a 2.2 GHz PC with 2 Gb of RAM.

3. Results

To provide an overall indication of the changes occurring in the relative opacity of the infant brain, the average photon detection rate (photons per second per active detector) was calculated for each set of data and for both source wavelengths. These values are plotted as a function of time in figure 3. The source power is approximately the same (13 mW) at the two wavelengths, and remained constant throughout the series of scans. The predefined detector attenuation values for each source/detector combination were identical for each dataset, and the surface coupling can also be assumed to have remained constant. Note, however, that smaller source–detector separations will still generally yield higher photon count rates, and therefore these globally averaged data inevitably give higher weight towards changes occurring within the outer regions of the brain.

As expected, increasing PaCO₂ causes higher global absorption due to increased CBV. There is a good apparent correlation between attenuation and PaCO₂, and detection rates recover to very similar values at the second baseline measurement recorded 140 min after the first. Meanwhile, the different characteristic absorption spectra of oxy- and deoxyhaemoglobin will cause any decrease in blood oxygenation at constant CBV to be manifested as an increase in attenuation at 780 nm and a decrease in attenuation at 815 nm. This effect is evident in the changes in photon detection rate occurring at both 95 min and 165 min.

As mentioned above, each of the four pairs of data listed in table 2 was used to generate difference images. However, in one case it was not possible to produce a stable reconstruction; the datasets 5 and 6 acquired at maximum PaCO₂ inevitably involve very low overall photon count rates, and the differences were too dominated by noise to facilitate generation of

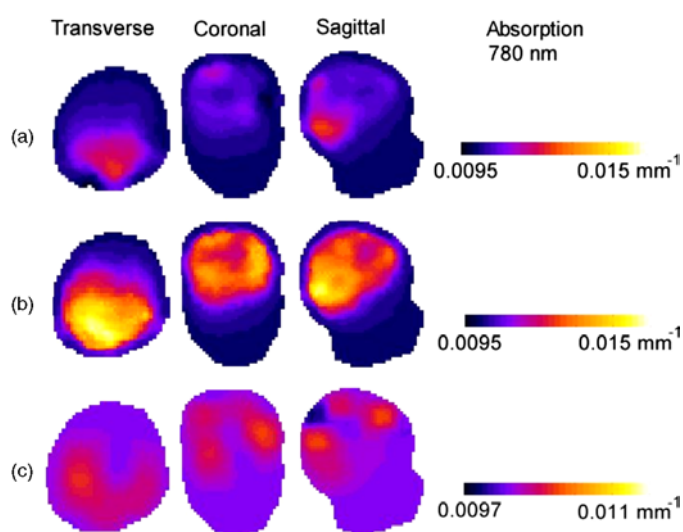


Figure 4. Transverse, coronal and sagittal slices across the 3D images of the infant head, representing differences in absorption at 780 nm, and corresponding to (a) baseline data acquired 140 min apart, (b) increased PaCO₂ at baseline PaO₂ and (c) decreased PaO₂ at baseline PaCO₂.

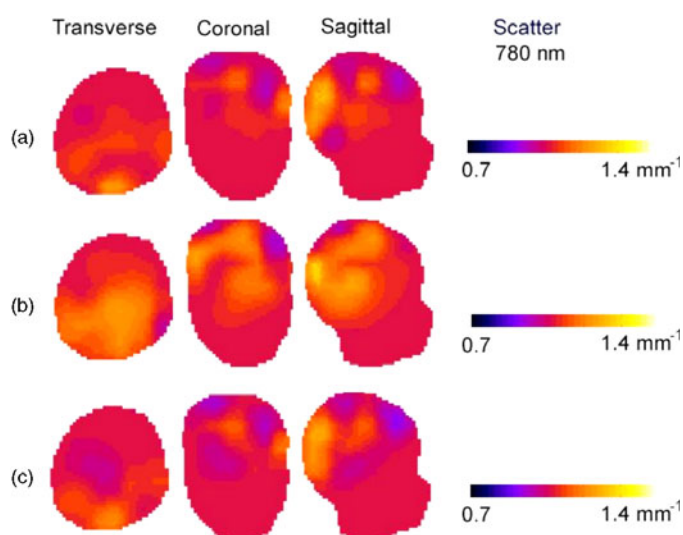


Figure 5. Transverse, coronal and sagittal slices across the 3D images of the infant head, representing differences in scatter at 780 nm, and corresponding to (a) baseline data acquired 140 min apart, (b) increased PaCO₂ at baseline PaO₂ and (c) decreased PaO₂ at baseline PaCO₂.

reliable images. In order to display the remaining 3D difference images we have extracted transverse, coronal and sagittal views across the infant head. The sagittal view corresponds to the anatomical midplane; the transverse view corresponds to the widest horizontal across the sagittal view and the coronal view corresponds to the midline between the top and the bottom of the transverse view. For the three pairs of data, the absorption and scatter images acquired at 780 nm are exhibited in figures 4 and 5, and the absorption and scatter images acquired at 815 nm are exhibited in figures 6 and 7. In other words, the top row of images in

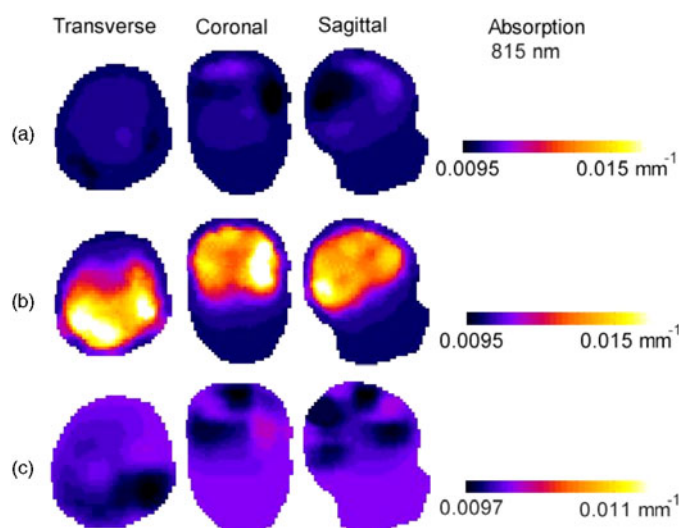


Figure 6. Transverse, coronal and sagittal slices across the 3D images of the infant head, representing differences in absorption at 815 nm, and corresponding to (a) baseline data acquired 140 min apart, (b) increased PaCO_2 and PaO_2 and (c) decreased PaO_2 at baseline PaCO_2 .

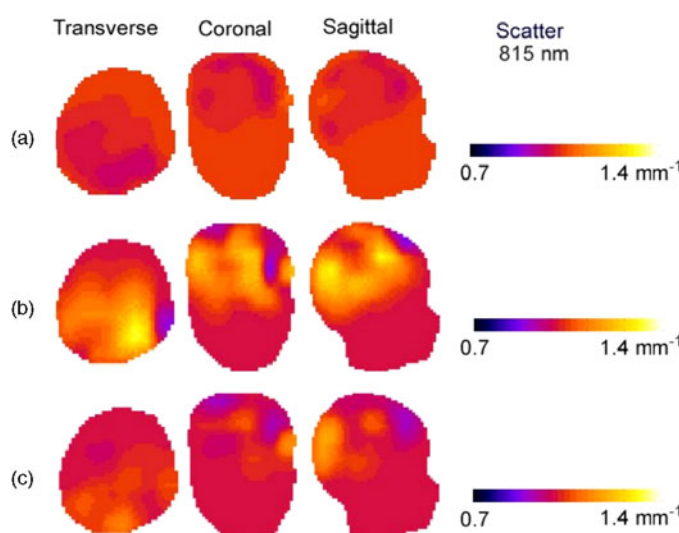


Figure 7. Transverse, coronal and sagittal slices across the 3D images of the infant head, representing differences in scatter at 815 nm, and corresponding to (a) baseline data acquired 140 min apart, (b) increased PaCO_2 and PaO_2 and (c) decreased PaO_2 at baseline PaCO_2 .

each figure corresponds to the difference in baseline data, the second row corresponds to the increased PaCO_2 and PaO_2 relative to the baseline, and the third row corresponds to the decreased oxygenation at baseline PaCO_2 . It is very important to note that all these images represent the perturbations in absorption and scatter superimposed on the homogeneous initial guess values. Thus a difference image generated from two identical sets of data would yield the initial guess itself, corresponding to $\mu'_s = 1.0 \text{ mm}^{-1}$ and $\mu_a = 0.01 \text{ mm}^{-1}$.

The baseline difference images provide a very valuable means of assessing the stability of the imaging system over a 140 min period between acquisitions, and of the potential manifestation of artefacts which might arise from the image reconstruction process. The absorption images reveal only very low contrast changes, largely confined to the rear of the left hemisphere, and probably show evidence of incomplete recovery of the infant CBV to normal following the earlier increase in PaCO₂. The scatter images are reasonably uniform, with displayed variation almost certainly due to residual cross talk between scatter and absorption, or possibly systematic artefact.

The difference images resulting from the increase in PaCO₂ from baseline to maximum confirm the large global increases in absorption at both wavelengths due to increased CBV. The coronal and transverse images show evidence of division into left and right hemispheres, and possibly of the blood-free ventricles within the centre. Sagittal and transverse images reveal a tendency for higher increases in absorption at the rear and left side of the brain, although the absence of sources and detectors near the eyes implies that frontal regions will be less well sampled. Lower absolute blood volume was exhibited within the frontal region of neonatal brain images published previously, although this could also be artefactual. The corresponding scatter difference images also indicate changes, although of reasonably small magnitude and almost certainly due to parameter cross talk. It should be noted that, if images are reconstructed with scatter held constant at the initial value, the absorption images are both quantitatively and qualitatively very similar.

The pattern of changes in the difference images corresponding to the decrease in PaO₂ at baseline PaCO₂ is much more subtle by comparison. At 780 nm, the absorption image reveals a modest increase in absorption, particularly at the rear and sides of the brain, while at 815 nm we observe slight decreases in absorption within localized regions. However, these oxygenation-change images may also be influenced by residual fluctuation in CBV, as the value of PaCO₂ was only held constant within a tolerance of ± 0.1 kPa. A small change in CBV can, of course, cause the overall absorption at the two wavelengths to change in the same direction. The scatter difference images for the oxygenation changes at both wavelengths are again small, and probably any displayed features are due to imperfect separation between scatter and absorption.

If oxy- and deoxyhaemoglobin are assumed to be the only absorbing compounds in the tissue (or if the contribution of other chromophores, such as water, can be estimated accurately), then images representing the absolute values of absorption coefficient at two wavelengths are sufficient to generate images corresponding to the volume of haemoglobin and the fractional oxygenation. This has been attempted previously using absolute absorption images of the infant brain derived with the aid of a homogeneous reference measurement (Hebden *et al* 2002). However, it is not possible to separate haemoglobin volume and fractional oxygenation using *differences* in absorption (Hillman 2002), and neither is it possible to derive the *change* in fraction oxygenation without knowledge of the absolute volume of haemoglobin. Nevertheless, images representing differences in absorption do permit images of changes in [Hb] and [HbO₂] to be derived, again assuming the contribution of other chromophores is known. The images shown in figures 8 and 9 were generated using the known extinction coefficients of both forms of haemoglobin, a haemoglobin concentration of whole blood of 2.37 mM derived from venous samples taken from the infant, and a fixed background absorption of 0.003 mm⁻¹ at both wavelengths. The background value is based on near-infrared measurements by van der Zee (1993) which indicated that other chromophores contribute about 30% of the total absorption in the newborn infant head. The top rows of figures 8 and 9 show the changes in [Hb] and [HbO₂] respectively due to the increase in PaCO₂ from baseline to maximum, and an increase in PaO₂. This reveals a substantial increase in [HbO₂], particularly within the sides

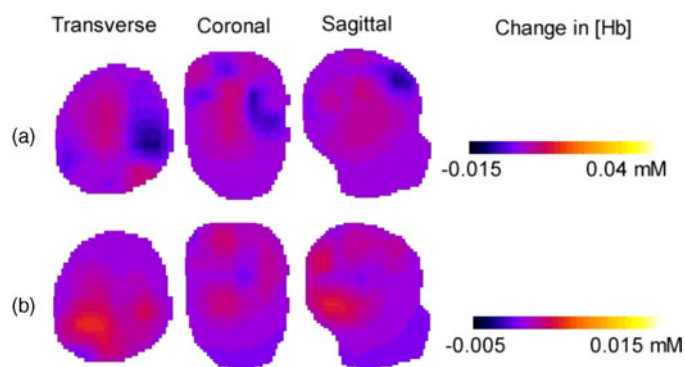


Figure 8. Transverse, coronal and sagittal slices revealing differences in deoxyhaemoglobin concentration corresponding to (a) increased PaCO_2 and PaO_2 , and (b) decreased PaO_2 at baseline PaCO_2 .

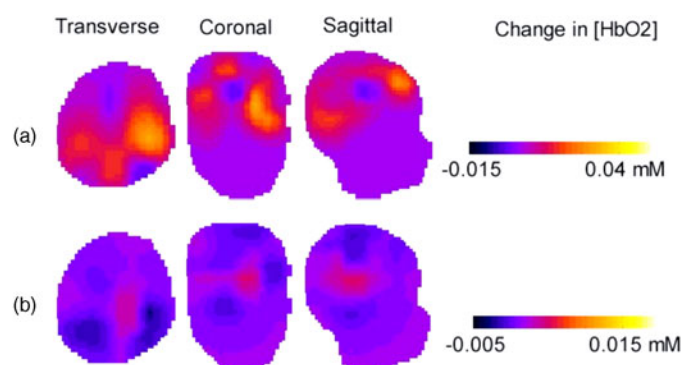


Figure 9. Transverse, coronal and sagittal slices revealing differences in oxyhaemoglobin concentration corresponding to (a) increased PaCO_2 and PaO_2 , and (b) decreased PaO_2 at baseline PaCO_2 .

and rear of the brain, but almost no overall change in [Hb]. A strong left–right asymmetry is also evident, although there are insufficient additional data to establish whether this relates to the physiological state of the infant or is purely artefact. The second rows of figures 8 and 9 show the corresponding changes due to the decrease in PaO_2 at baseline PaCO_2 . As expected, we observe an overall decrease in $[\text{HbO}_2]$ and increase in [Hb]. Again, it is possible that these images are influenced to some degree by the residual fluctuation in CBV.

4. Discussion

Imaging isolated regions of contrasting optical properties in an otherwise uniform volume is a popular method of evaluating optical tomography techniques, and has been widely demonstrated using a variety of phantoms (Dehghani *et al* 2003, Hebden *et al* 2001, O’Leary *et al* 1995, Pei *et al* 2001). Researchers often utilize data recorded with and without the contrasting objects, which is straightforward to obtain using liquid-based phantoms. As described earlier in section 2.2, this difference imaging approach provides a means of calibrating for certain system- and geometry-dependent factors. A further benefit of this approach is that it yields readily to linear image reconstruction techniques (O’Leary *et al*

1995). However, researchers are also applying difference imaging to *in vivo* studies where a uniform background cannot be assumed. As shown here, suitable data can be obtained by inducing a local change in the tissue optical properties. A further example of this method was demonstrated by Bluestone *et al* (2001), who employed optical tomography to visualize changes in cerebral oxygenation induced by the Valsalva manoeuvre. Another means of obtaining difference data is to utilize an extrinsic contrast agent. For example, a perturbative approach was exploited by Intes *et al* (2003) to acquire images of the breast which display the distribution of the near-infrared absorbing agent indocyanine green, injected intravenously.

Acquiring an accurate image using difference data still requires that the image reconstruction algorithm knows or can model the distribution of light within the tissue. This requires an estimate of the initial (or 'background') optical properties of the tissue, and in the absence of prior information it is generally assumed that these are uniform. Nevertheless, the distribution of scatter and absorption within the infant brain is far from uniform. A further assumption inherent in the linear perturbation approach is that the detected photons will have travelled through identical regions of the head for both sets of data from which differences are calculated. If the difference in optical properties is sufficiently large, then obviously the distributions of photons within the volume will be significantly different, and so the difference imaging method becomes invalid. Arridge and Schweiger (1995) have used simulations to show that a linearized reconstruction starting from a uniform initial guess can fail to produce an accurate difference image from datasets where neither corresponds to a homogeneous object. Overall, it is evident that the application of difference imaging to real tissues has to be treated with some caution.

The difference images we present here will be influenced in a complicated (and so far largely unexplored) way by the absolute distribution of scatter and absorption within the infant brain. True difference images can, of course, be generated by first generating absolute images. While acquiring absolute images represents the ultimate objective of our work, and with some success already demonstrated (Hebden *et al* 2002), this still represents a very difficult problem, which is hindered by the lack of absolute integrated intensity measurements for reasons described in section 2.2. The employment of intensity difference information in the reconstruction provided scatter difference images here which contain significantly less artefact than the absolute scatter images acquired previously. However, these scatter differences appear to exhibit little that does not correlate with the absorption changes, and therefore are very likely due to residual parameter cross talk. The inability to reconstruct reliable images of the oxygenation change at high PaCO₂ underlines the inevitable limitations of 3D optical tomography when the overall signals are very low. Clearly, future work must include studies to determine the sensitivity of the technique as a function of the magnitude of the available signal.

Encouragingly, the baseline absorption difference images appear free from major artefact. However, this itself does not represent a robust justification for the difference imaging method, since a uniform difference image implies nothing more than the two sets of data are similar, and not that we have extracted anything meaningful about the internal structure of optical properties of the infant brain. The brain images generated using the induced changes in PaO₂ and PaCO₂ are generally in accordance with what should be expected, although it is important to note that the physiological responses of this severely brain injured infant cannot be expected to be those of a normal infant, and in fact remain largely unknown. Studies such as these provide the first steps towards gaining a greater understanding about the neuro-physiological consequences of severe asphyxia-ischaemia. The images representing the changes in [Hb] and [HbO₂] resulting from the variation in PaCO₂ and in PaO₂ are in accordance with the expected physiological response. However, the fact that there are no alternative imaging data

with which to compare and validate these results underlines the difficulty of obtaining this information from infants in intensive care, and highlights the potentially important role of optical tomography. Nevertheless, magnetic resonance imaging (MRI) can be used to observe changes in cerebral blood volume and [Hb] in infants, and simultaneous optical/MRI studies are planned which we anticipate will provide appropriate validation.

The propagation of light through the non-scattering regions of cerebral-spinal fluid (CSF), which normally surround the brain and fill the ventricles, is expected to be a serious potential source of error in the reconstruction of 'absolute' images of optical parameters due to the failure of a diffusion-based algorithm to accommodate such regions in the forward model. However, the extent to which such regions may affect difference imaging, where the regions exist in the same place for both sets of data, is less certain, but the effect is generally assumed to be less severe if not negligible. This is certainly the finding of Pei *et al* (2001) whose imaging system is based on continuous intensity measurements. The influence of such regions on images reconstructed from time-resolved data is currently subject to a series of experimental investigations at UCL using appropriate phantoms. Since TOAST can only reconstruct what the forward model is capable of representing, significantly more complex models are being sought, including the incorporation of anisotropic-scattering (Heino *et al* 2003) and non-scattering (Riley *et al* 2000) regions. Work is also being conducted to significantly enhance reconstruction speed and accuracy by employing specific *a priori* information (e.g., from an MRI, CT or ultrasound scan of the individual infant) when available. While these and other technical problems still need to be solved, the results presented above demonstrate that 3D optical tomography of the infant brain is getting closer to becoming the vital imaging tool that doctors working with this most vulnerable of patient groups urgently require.

Acknowledgments

Support for this work has been generously provided by the Wellcome Trust, Action Research and the EPSRC.

References

- Arridge S R 1999 Optical tomography in medical imaging *Inverse Problems* **15** R41–R93
- Arridge S R and Schweiger M 1995 Sensitivity to prior knowledge in optical image reconstruction *Proc. SPIE* **2389** 378–88
- Arridge S R and Schweiger M 1997 Image reconstruction in optical tomography *Phil. Trans.R. Soc. Lond. B* **352** 717–26
- Benaron D A, Hintz S R, Villringer A, Boas D, Kleinschmidt A, Frahm J, Hirth C, Obrig H, van Houten J C, Kermit E L, Cheong W-F and Stevenson D K 2000 Noninvasive functional imaging of human brain using light *J. Cereb. Blood Flow Metab.* **20** 469–77
- Bluestone A Y, Abdoulaev G, Schmitz C H, Barbour R L and Hielscher A H 2001 Three-dimensional optical tomography of hemodynamics in the human head *Opt. Exp.* **9** 272–86
- Brazy J E, Darrell V, Lewis M D, Mitnick M H and Jöbsis F F 1985 Noninvasive monitoring of cerebral oxygenation in preterm infants: preliminary observations *Pediatrics* **75** 217–25
- Chance B, Anday E, Nioka S, Zhou S, Hong L, Worden K, Li C, Murray T, Ovetsky Y, Pidikiti D and Thomas R 1998 A novel method for fast imaging of brain function, non-invasively, with light *Opt. Exp.* **2** 411–23
- Dehghani H, Pogue B W, Shudong J, Brooksby B and Paulsen K D 2003 Three-dimensional optical tomography: resolution in small-object imaging *Appl. Opt.* **42** 3117–28
- Edwards A D, Wyatt J S, Richardson C, Delpy D T, Cope M and Reynolds E O R 1988 Cotside measurement of cerebral blood flow in ill newborn infants by near infrared spectroscopy *Lancet* **2** 770–1
- Gibson A P, Riley J, Schweiger M, Hebden J C, Arridge S R and Delpy D T 2003 A method for generating patient-specific finite elements meshes for head modelling *Phys. Med. Biol.* **48** 481–96
- Hebden J C 2003 Advances in optical imaging of the newborn infant brain *Psychophysiology* **40** 501–10

- Hebden J C, Gibson A, Yusof R Md, Everdell N, Hillman E M C, Delpy D T, Arridge S R, Austin T, Meek J H and Wyatt J S 2002 Three-dimensional optical tomography of the premature infant brain *Phys. Med. Biol.* **47** 4155–66
- Hebden J C, Gonzalez F M, Gibson A, Hillman E M C, Yusof R Md, Everdell N, Delpy D T, Zaccanti G and Martelli F 2003 Assessment of an *in situ* temporal calibration method for time-resolved optical tomography *J. Biomed. Opt.* **8** 87–92
- Hebden J C, Veenstra H, Dehghani H, Hillman E M C, Schweiger M, Arridge S R and Delpy D T 2001 Three dimensional time-resolved optical tomography of a conical breast phantom *Appl. Opt.* **40** 3278–87
- Heino J, Arridge S R, Sikora J and Somersalo E 2003 Anisotropic effects in highly scattering media *Phys. Rev. E* **68** Article number 31908
- Hillman E M C 2002 Experimental and theoretical investigations of near infrared tomographic imaging methods and clinical applications *PhD Thesis* University of London (<http://www.medphys.ucl.ac.uk/research/borg/theses.htm>)
- Hillman E M C, Hebden J C, Schmidt F E W, Arridge S R, Schweiger M, Dehghani H and Delpy D T 2000 Calibration techniques and datatype extraction for time-resolved optical tomography *Rev. Sci. Instrum.* **71** 3415–27
- Hintz S R, Benaron D A, van Houten J P, Duckworth J L, Liu F W H, Spilman S D, Stevenson D K and Cheong W-F 1998 Stationary headband for clinical time-of-flight optical imaging at the bedside *Photochem. Photobiol.* **68** 361–9
- Hintz S R, Benaron D A, Siegal A M, Zourabian A, Stevenson D K and Boas D A 2001 Bedside functional imaging of the premature infant brain during passive motor activation *J. Perinat. Med.* **29** 335–43
- Hintz S R, Cheong W-F, van Houten J P, Stevenon D K and Benaron D A 1999 Bedside imaging of intracranial hemorrhage in the neonate using light: comparison with ultrasound, computed tomography, and magnetic resonance imaging *Pediatr. Res.* **45** 54–9
- Intes X, Ripoll J, Chen Y, Nioka S, Yodh A G and Chance B 2003 *In vivo* continuous-wave optical breast imaging enhanced with Indocyanine Green *Med. Phys.* **30** 1039–2047
- Isobe K, Kasuka T, Fujikawa Y, Kondo M, Kawada K, Yasuda S, Itoh S, Hirao K and Onishi S 2000 Changes in cerebral hemoglobin concentration and oxygen saturation immediately after birth in the human neonate using full-spectrum near infrared spectroscopy *J. Biomed. Opt.* **5** 283–6
- Isobe K, Kasuka T, Nagano K, Okubo K, Yasuda S, Kondo M, Itoh S and Onishi S 2001 Functional imaging of the brain in sedated newborn infants using near infrared topography during passive knee movement *Neurosci. Lett.* **299** 221–4
- Jöbsis F F 1977 Noninvasive, infrared monitoring of cerebral and myocardial oxygen sufficiency and circulatory parameters *Science* **198** 1264–7
- Meek J H, Elwell C E, McCormick D C, Edwards A D, Townsend J P, Stewart A L and Wyatt J S 1999 Abnormal cerebral haemodynamics in perinatally asphyxiated neonates related to outcome *Arch. Dis. Child. Fetal Neonatal Ed.* **81** F110–F115
- O'Leary M A, Boas D A, Chance B and Yodh A G 1995 Experimental Images of heterogeneous turbid media by frequency-domain diffusing-photon tomography *Opt. Lett.* **20** 426–8
- Pei Y, Graber H L and Barbour R L 2001 Normalized-constraint algorithm for minimizing inter-parameter crosstalk in DC optical tomography *Opt. Exp.* **9** 97–109
- Reynolds E O R, Wyatt J S, Azzopardi D, Delpy D T, Cady E B, Cope M and Wray S 1988 New non-invasive methods for assessing brain oxygenation and haemodynamics *Br. Med. Bull.* **44** 1052–75
- Riley J, Dehghani H, Schweiger M, Arridge S R, Ripoll J and Nieto-Vesperinas M 2000 3D Optical tomography in the presence of void regions *Opt. Exp.* **7** 462–7
- Schmidt F E W, Fry M E, Hillman E M C, Hebden J C and Delpy D T 2000 A 32-channel time-resolved instrument for medical optical tomography *Rev. Sci. Instrum.* **71** 256–65
- Schweiger M and Arridge S R 1999 Application of temporal filters to time resolved data in optical tomography *Phys. Med. Biol.* **44** 1699–717
- Skov L L, Pryds O and Griesen G 1991 Estimating cerebral blood flow in newborn infants: comparison of near infrared spectroscopy and ¹³³xenon clearance *Pediatr. Res.* **30** 570–3
- Tsuji M, Saul J P, du Plessis A, Eichenwald E, Sobh J, Crocker R and Volpe J 2000 Cerebral intravascular oxygenation correlates with mean arterial pressure in critically ill premature infants *Pediatrics* **106** 625–32
- van der Zee P 1993 Measurement and modelling of the optical properties of human tissue in the near infrared *PhD Thesis* University of London
- Wyatt J S 1993 Near infrared spectroscopy in asphyxial brain injury *Clinics Perinatol.* **20** 369–78